

InfoMax-GAN: Improved Adversarial Image Generation via Information Maximization and Contrastive Learning

Kwot Sin Lee Ngoc-Trung Tran Ngai-Man Cheung

Abstract—While Generative Adversarial Networks (GANs) are fundamental to many generative modelling applications, they suffer from numerous issues. In this work, we propose a principled framework to simultaneously address two fundamental issues in GANs: catastrophic forgetting of the discriminator and mode collapse of the generator. We achieve this by employing for GANs a contrastive learning and mutual information maximization approach, and perform extensive analyses to understand sources of improvements. Our approach significantly stabilizes GAN training and improves GAN performance for image synthesis across five datasets under the same training and evaluation conditions against state-of-the-art works. Our approach is simple to implement and practical: it involves only one auxiliary objective, has low computational cost, and performs robustly across a wide range of training settings and datasets *without any hyperparameter tuning*. For reproducibility, our code is available at <https://github.com/kwotsin/mimicry>.

Index Terms—Generative Adversarial Networks, Contrastive Learning, Information Maximization, Image Synthesis

I. INTRODUCTION

The field of generative modelling has witnessed incredible successes since the advent of Generative Adversarial Networks (GANs) [1], a form of generative model known for its sampling efficiency in generating high-fidelity data [2]. In general, a GAN tries to model the true data distribution of a finite amount of empirical data, and is composed of two models: a generator and a discriminator. The modelling of the distribution is achieved as both models play an adversarial minimax game where the generator tries to fool the discriminator with some fake data generated from sampling a noise prior, and the discriminator tries to avoid being fooled by correctly classifying a given sample as real or fake. This adversarial game is captured by the following equation:

$$\min_G \max_D V(D, G) = \mathbb{E}_{x \sim p_r(x)} [\log D(x)] + \mathbb{E}_{z \sim p(z)} [\log(1 - D(G(z)))] \quad (1)$$

where V is the value function, $p(z)$ is a prior noise distribution, $p_r(x)$ is the real data distribution, and $G(z)$ represents the generated data after passing some randomly sampled noise z through the generator G .

In this minimax formulation, training the discriminator and generator with their respective minimax loss functions aims

to minimize the Jensen-Shannon (JS) divergence between the real and generated data distributions [1] p_r and p_g respectively. However, GAN training is notoriously difficult. Firstly, such theoretical guarantees only come under the assumption of the discriminator being trained to optimality [3], which may lead to saturating gradients in practice. Even so, there is no guarantee for convergence in this minimax game as both generator and discriminator are simultaneously and independently finding a Nash equilibrium in a high-dimensional space. Finally, GANs face the perennial problem of mode collapse, where p_g collapses to only cover a few modes of p_r , resulting in generated samples of limited diversity. Consequently, recent years have seen efforts [4]–[10] to mitigate these GAN problems, including using gradient matching [5] and a two time-scale update rule [7].

A primary cause of GAN training instability stems from the non-stationary nature of the training environment: as the generator learns, the modeled distribution p_g the discriminator faces is ever changing. As we represent our GAN models as neural networks, the discriminator neural network is susceptible to *catastrophic forgetting* [11]–[14], a situation where the network forgets about prior tasks in order to focus on the current one as the weights of the network updates, which ultimately contributes to training instability. The state-of-the-art Self-supervised GAN (SSGAN) [12] is the first to demonstrate that a representation learning approach could mitigate discriminator catastrophic forgetting, thus improving training stability. However, the approach still does not explicitly mitigate *mode collapse*, and has a failure mode in image generation on datasets involving domains like faces [12]. To address these problems, we present an approach to simultaneously mitigate catastrophic forgetting and mode collapse in GANs, and demonstrate a wide range of practical improvements on natural image synthesis using GANs.

We summarize our contributions below:

- We present a GAN framework for improving natural image synthesis through simultaneously mitigating two key GAN issues using just one objective: catastrophic forgetting of the discriminator (via information maximization) and mode collapse of the generator (via contrastive learning). Our approach addresses issues in both discriminator and generator, rather than either alone. We perform analyses to substantiate these claims and demonstrate our framework’s effectiveness.
- With this multi-faceted approach, we demonstrate our framework can significantly improve GAN image synthe-

K.S. Lee is with University of Cambridge, England, United Kingdom. Email: ksl36@cam.ac.uk

N.T. Tran and N.M. Cheung are with Singapore University of Technology and Design (SUTD), Singapore. Emails: {ngoctrung_tran, ngaiman_cheung}@sutd.edu.sg

sis across *five* different datasets against state-of-the-art works under the *same training and evaluation conditions*.

- Our framework is lightweight and practical: it introduces just one auxiliary objective, has low computational cost, and is robust against a wide range of training hyperparameters *without any tuning* required.
- Our work is the first to demonstrate the effectiveness of contrastive learning for significantly improving GAN performance, which we hope would open a new research direction in this area.

II. BACKGROUND

a) *Mutual information and representation learning*: The mutual information between two random variables X and Y with marginals $p(x)$ and $p(y)$ can be defined as the Kullback-Leibler (KL) divergence between their joint distribution and product of marginals:

$$\begin{aligned}\mathcal{I}(X; Y) &= \mathcal{D}_{\text{KL}}(p(x, y) || p(x)p(y)) \\ &= \int_X \int_Y p(x, y) \log \frac{p(x, y)}{p(x)p(y)} dy dx\end{aligned}\quad (2)$$

Intuitively, for some random variable Y that is independent of X , we have $p(x, y) = p(x)p(y)$, rendering the log term to be 0 and thus $\mathcal{I}(X; Y) = 0$. Viewed from this perspective, mutual information is non-negative and represents the amount of information one gains about a random variable from the knowledge of another random variable.

While mutual information is a straightforward concept, it has been strongly tied to representation learning [15], where we aim to learn an encoder function E that ideally captures the most important features of the input data X , often at a lower dimensional latent space. This concept is encapsulated by the InfoMax objective [16]:

$$\max_{E \in \mathcal{E}} \mathcal{I}(X; E(X)) \quad (3)$$

where \mathcal{E} is some function class, and the objective is to find some E that maximizes the mutual information between the input data and its encoded representations $E(X)$. To maximize on the InfoMax objective, one could alternatively maximize $\mathcal{I}(C_\psi(X); E_\psi(X))$, where C_ψ and E_ψ are encoders part of the same architecture parameterised by ψ . It can be shown in [17] maximizing $\mathcal{I}(C_\psi(X); E_\psi(X))$ is maximizing on a lower bound of the InfoMax objective:

$$\mathcal{I}(C_\psi(X); E_\psi(X)) \leq \mathcal{I}(X; (C_\psi(X), E_\psi(X))) \quad (4)$$

In practice, as noted in [17], [18], maximizing $\mathcal{I}(C_\psi(X); E_\psi(X))$ has several advantages: (a) Using different feature encodings allow us to capture different views and modalities of the data for flexibility of modelling [19], [20]; (b) The encoded data lies in a much lower dimensional latent space than that of the original data, thus reducing computational constraints.

b) *Contrastive learning*: An emerging theme in recent state-of-the-art works in unsupervised representation learning [19]–[25] lies in taking a contrastive approach to maximizing the mutual information between encoded local and global features. Yet, since directly maximizing mutual information is

often intractable in practice [26], these works often maximize on the InfoNCE [21] lower bound instead, which involves a contrastive loss minimized through having a critic correctly finding a positive sample in contrast to a set of negative samples. Such positive/negative samples can be arbitrarily created by pairing features [22], augmentation [27], or a combination of both [19]. Our work similarly maximizes on this InfoNCE bound, and most closely follows the Deep InfoMax [22] approach of obtaining local and global features for the maximization, for which the reader is highly encouraged to read.

III. INFOMAX-GAN

In this section, we first explain our approach and its benefits in alleviating two key issues of GANs.

A. Approach

Figure 1 illustrates the InfoMax-GAN framework, which performs contrastive learning and information maximization simultaneously in a GAN setting. Firstly, to maximize on the lower bound of the InfoMax objective, $\mathcal{I}(C_\psi(X); E_\psi(X))$, we set E_ψ to represent layers of a GAN discriminator leading to the global features, and C_ψ as layers leading to the local features. Here, $C_\psi = C_{\psi,1} \circ \dots \circ C_{\psi,n}$ represents a series of n intermediate discriminator layers leading to the last local feature map $C_\psi(x)$ and f_ψ is the subsequent layer transforming $C_\psi(x)$ to a global feature vector $E_\psi(x)$, which is ultimately used for computing the GAN objective \mathcal{L}_{gan} . In our work, the local and global features are always the penultimate and final feature outputs of the discriminator encoder respectively, and we subsequently ablate this effect by comparing with alternative designs.

Next, the local/global features $C_\psi(x)$ and $E_\psi(x)$ are extracted from the discriminator and passed to the critic networks ϕ_θ and ϕ_ω to be projected to a higher dimension Reproducing Kernel Hilbert Space (RKHS) [28], which exploits the value of using linear evaluation to capture similarities between the global and local features. These projected features undergo a Contrastive Pairing phase to create the positive and negative samples. In this phase, given some image x , a positive sample is created by pairing the (projected) global feature vector $\phi_\omega(E_\psi(x))$ with a (projected) local spatial vector $\phi_\theta(C_\psi^{(i)}(x))$ from the image's own (projected) local feature map $\phi_\theta(C_\psi(x))$, where $i \in \mathcal{A} = \{0, 1, \dots, M^2 - 1\}$ is an index to the $M \times M$ local feature map. Doing so, our resulting positive sample is the pair $(\phi_\theta(C_\psi^{(i)}(x)), \phi_\omega(E_\psi(x)))$ for some i . For each of such positive sample, our negative samples are obtained by sampling local spatial vectors from the projected local feature map of another image x' from the same mini-batch, and can be represented as the pairs $(\phi_\theta(C_\psi^{(i)}(x')), \phi_\omega(E_\psi(x)))$. Intuitively, in this step, we constrain the discriminator to produce global features of some image that maximizes mutual information with the local features of the same image, rather than those from other images.

In fact, we can take a step further by also considering for each positive sample, the pairs $(\phi_\theta(C_\psi^{(j)}(x)), \phi_\omega(E_\psi(x)))$, $j \in \mathcal{A}, j \neq i$ as negative samples. That is, we use other spatial

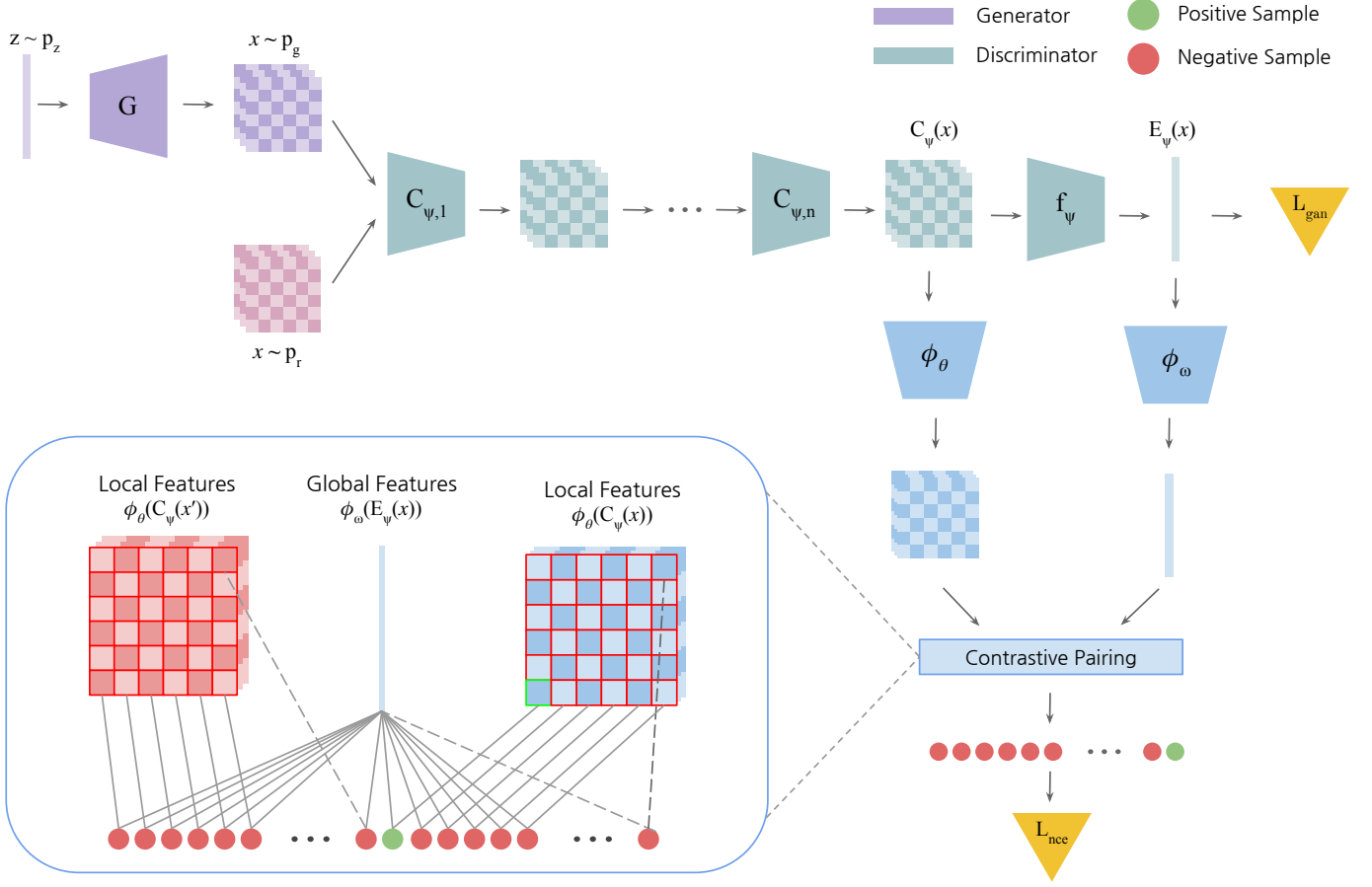


Fig. 1: Illustration of the InfoMax-GAN framework. An image x is sampled from the real data distribution p_r or fake data distribution p_g as modeled by the generator G . Image x passes through a discriminator encoder $E_{\psi} = f_{\psi} \circ C_{\psi}$, where $C_{\psi} = C_{\psi,1} \circ \dots \circ C_{\psi,n}$ is a series of n intermediate discriminator layers leading to the last local feature map $C_{\psi}(x)$ and f_{ψ} transforms $C_{\psi}(x)$ to a global feature vector $E_{\psi}(x)$, which is subsequently used to compute the GAN objective L_{gan} . The local and global features $C_{\psi}(x)$ and $E_{\psi}(x)$ are then projected to a higher dimension by the critic networks ϕ_{θ} and ϕ_{ω} respectively. Finally, the resulting features undergo a Contrastive Pairing phase involving local features from another image x' , to produce positive and negative samples for computing the contrastive loss L_{nce} .

vectors from the *same* local feature map to create negative samples. Doing so, we regularize the learnt representations to avoid trivial solutions to the mutual information maximization objective, since the global features is constrained to have consistently high mutual information with *all* spatial vectors of its own local feature map, rather than from only select spatial vectors. For instance, a trivial objective can be achieved if the global features only have high mutual information with only some local spatial vectors representing the background, which can be easy to achieve when the background has consistent color and texture. Through this regularization, the global features would effectively aggregate local information from all parts of the image to be representative of the image.

Thus, in total, for N images in a mini-batch, we can produce positive and negative samples to perform an NM^2 way classification for each positive sample. Through this contrastive learning approach, it can be shown in [21] one maximizes the InfoNCE lower bound of the mutual information $\mathcal{I}(C_{\psi}(X); E_{\psi}(X))$.

Formally, for some set of N random images $X =$

$\{x_1, \dots, x_N\}$ and set $\mathcal{A} = \{0, 1, \dots, M^2 - 1\}$ representing indices of a $M \times M$ spatial sized local feature map, we can represent the contrastive loss as:

$$\begin{aligned} \mathcal{L}_{nce}(X) &= -\mathbb{E}_{x \in X} \mathbb{E}_{i \in \mathcal{A}} \left[\log p(C_{\psi}^{(i)}(x), E_{\psi}(x) | X) \right] \\ &= -\mathbb{E}_{x \in X} \mathbb{E}_{i \in \mathcal{A}} [\Delta] \\ \Delta &= \log \frac{\exp(g_{\theta, \omega}(C_{\psi}^{(i)}(x), E_{\psi}(x)))}{\sum_{(x', i) \in X \times \mathcal{A}} \exp(g_{\theta, \omega}(C_{\psi}^{(i)}(x'), E_{\psi}(x)))} \end{aligned} \quad (5)$$

where $g_{\theta, \omega} : \mathbb{R}^{1 \times 1 \times K} \times \mathbb{R}^{1 \times 1 \times K} \rightarrow \mathbb{R}$ is a critic mapping the local and global features to a scalar score, for some local and global feature vectors with K dimensions. Formally, we can define $g_{\theta, \omega}$ to be:

$$g_{\theta, \omega}(C_{\psi}^{(i)}(x), E_{\psi}(x)) = \phi_{\theta}(C_{\psi}^{(i)}(x))^T \phi_{\omega}(E_{\psi}(x)) \quad (6)$$

where $\phi_{\theta} : \mathbb{R}^{M \times M \times K} \rightarrow \mathbb{R}^{M \times M \times R}$ and $\phi_{\omega} : \mathbb{R}^{1 \times 1 \times K} \rightarrow \mathbb{R}^{1 \times 1 \times R}$ are the critic networks parameterized by θ and ω respectively, projecting the local and global features to the

higher Reproducing Kernel Hilbert Space (RKHS). In practice, ϕ_θ and ϕ_ω are defined as shallow networks with only 1 hidden layer following [22], but with spectral normalized weights as well. These shallow networks serve to only project the feature dimensions of the input features, and preserve their original spatial sizes.

To stabilize training, we constrain the discriminator to learn from only the contrastive loss of real image features, and similarly for the generator, from only the contrastive loss of fake image features. We formulate the losses for discriminator and generator \mathcal{L}_D and \mathcal{L}_G as such:

$$\mathcal{L}_G = \mathcal{L}_{\text{gan}}(\hat{D}, G) + \alpha \mathcal{L}_{\text{ncc}}(X_g) \quad (7)$$

$$\mathcal{L}_D = \mathcal{L}_{\text{gan}}(D, \hat{G}) + \beta \mathcal{L}_{\text{ncc}}(X_r) \quad (8)$$

where α and β are hyperparameters; \hat{D} and \hat{G} represent a fixed discriminator and generator respectively; X_r and X_g represent sets of real and generated images respectively; and \mathcal{L}_{gan} is the hinge loss for GANs [29]:

$$\begin{aligned} \mathcal{L}_{\text{gan}}(D, \hat{G}) = & \mathbb{E}_{x \sim p_r} [\min(0, 1 - D(x))] \\ & + \mathbb{E}_{z \sim p_z} [\min(0, 1 + D(\hat{G}(z)))] \end{aligned} \quad (9)$$

$$\mathcal{L}_{\text{gan}}(\hat{D}, G) = -\mathbb{E}_{z \sim p_z} [\hat{D}(G(z))] \quad (10)$$

In practice, we set $\alpha = \beta = 0.2$ for all experiments for simplicity, with ablation studies to show our approach is robust across a wide range of α and β values.

In summary, through information maximization, our approach improves the global feature representations that are subsequently used for the GAN training task, which not only provides more informative gradient feedback for training, but importantly mitigates the catastrophic forgetting problem of the discriminator. Through a contrastive learning approach for this maximization, our approach helps to mitigate mode collapse nature of the generator. In the next sections, we substantiate these claims.

B. Mitigating Catastrophic Forgetting

Our approach mitigates a key issue in GANs: *catastrophic forgetting* of the discriminator, a situation where due to the non-stationary nature of the training environment, the discriminator learns only ad-hoc representations and forget about prior tasks it was trained on. For instance, while the discriminator may learn to penalize flaws in global structures early in GAN training [12], it may later forget these relevant representations in order to learn those for finding detailed flaws in local structures, which overall contributes to training instability.

Inspired by [12], we examine the ability of our approach in mitigating catastrophic forgetting: we train a discriminator classifier on the one-vs-all CIFAR-10 classification task where the underlying class distribution changes every 1K iterations, and the cycle repeats every 10K iterations. As seen in Figure 2, without the InfoMax objective, the classifier can overfit to a certain class distribution and produce very low accuracy when the class distribution is changed. When training is regularized with the InfoMax objective, the classifier successfully remembers

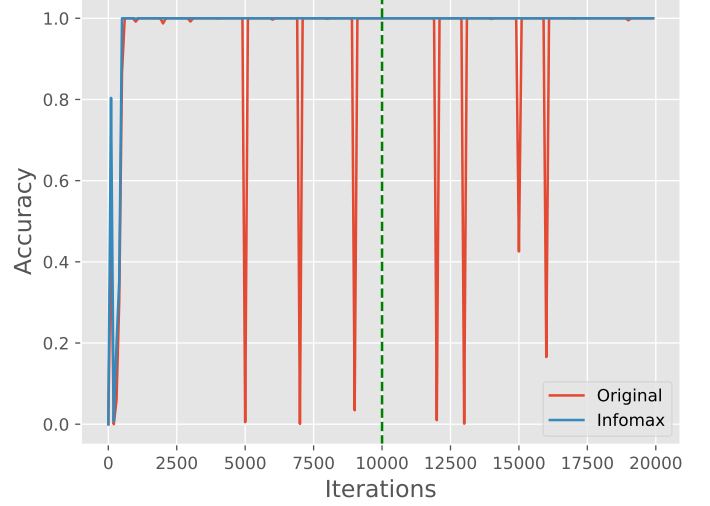


Fig. 2: Accuracy of a classifier when trained on the one-vs-all CIFAR-10 classification task. Regularized with the InfoMax objective by minimizing (5), the classifier successfully predicts classes trained from previous iterations even when the underlying class distribution changes.

all prior classes it was trained on. Thus, the InfoMax objective helps the discriminator to reduce catastrophic forgetting and adapt to the non-stationary nature of the generated image distribution, which ultimately stabilizes GAN training.

C. Mitigating Mode Collapse

Our approach also mitigates a persistent problem of the generator: *mode collapse*. For a fully mode collapsed generator, we have $x = x' \forall x, x' \sim X_g$, where X_g is a set of randomly generated images, such that $C_\psi(x) = C_\psi(x')$. This means the term $p(C_\psi^{(i)}(x), E_\psi(x) | X_g)$ approaches 0 in the limit, rather than the optimal value 1, as the critics are not able to distinguish apart the multiple identical feature pairs from individual images.

To validate this, we show there is a direct correlation between the diversity of generated images and the contrastive learning task accuracy $p(C_\psi^{(i)}(x), E_\psi(x) | X)$. We train the discriminator to solve the contrastive task using CIFAR-10 training data, and simulate 3 different kinds of generators using CIFAR-10 test data: (a) a perfect generator with no mode collapse that can generate *all classes of images*; (b) a partially mode collapsed generator that can only generate *one class of images* and (c) a totally mode collapsed generator that can only generate *one image*.

From Figure 3a, we observe a perfect generator with no mode collapse best solves the contrastive task, and a partially mode collapsed generator has a consistently poorer accuracy in the contrastive task than the perfect generator. This concurs with our expectation: images from only one class exhibit a much lower diversity than images from all classes, and so distinguishing the positive samples amongst similar and harder negative samples results in greater difficulty in solving the contrastive task. Furthermore, for a totally mode collapsed generator which can only generate one image, we observe the

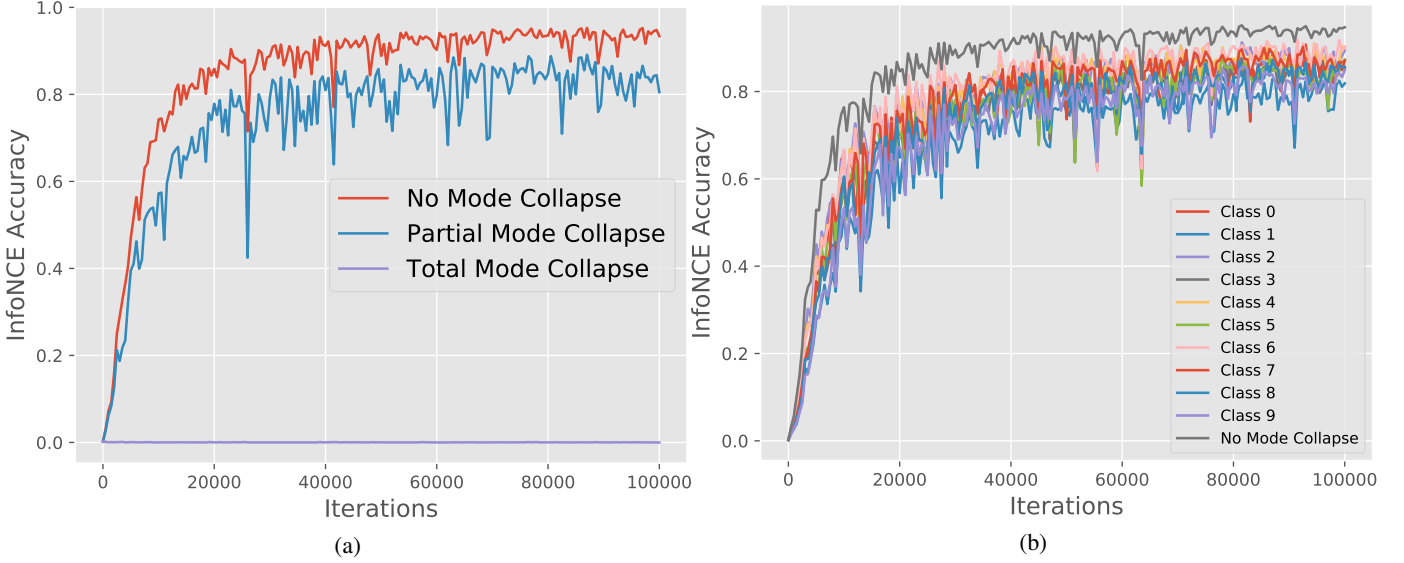


Fig. 3: Contrastive task accuracy when simulating generators exhibiting a range of mode collapse behaviours using CIFAR-10 data. (a) We show that the less mode collapsed a generator is, the better the accuracy for contrastive task. (b) The contrastive task accuracy is consistently lower when the generator has partially mode collapsed to any individual class, compared to when there is no mode collapse.

accuracy is *near zero*, which confirms our initial hypothesis. For any N images, there are NM^2 samples to classify in the contrastive task, with $NM^2 - 1$ negative samples for each positive sample. However, if all N images are identical due to total mode collapse, then there exists $N - 1$ negative samples identical to each positive sample, which makes the contrastive task nearly impossible to solve. Thus, to solve the contrastive task well, the generator is highly encouraged to generate images with greater diversity, which reduces mode collapse.

Furthermore, from Figure 3b, we see the performance of any individual class demonstrating partial mode collapse is *consistently worse* than the case of no mode collapse, where all classes of images are used. Thus, the generator is incentivised to not collapse to producing just any one class that can fool the discriminator easily, since producing *all classes* of images would naturally lead to the best performance in the contrastive task.

IV. EXPERIMENTS

A. GAN Architectures

To evaluate our approach, we experiment with Spectral Normalization GAN (SNGAN) [29] and the state-of-the-art Self-supervised GAN (SSGAN) [12]. SNGAN is an unconditional GAN utilizing spectral normalization to stabilize GAN training by constraining the discriminator to be 1-Lipschitz, and has been the basis of recent state-of-the-art GANs [30]–[33]. SSGAN is the state-of-the-art unconditional GAN that has achieved a highly competitive performance compared to conditional GANs of the same architectural capacity. SSGAN does not utilise human-annotated labels, but performs 4 different rotations on the images to obtain pseudo-labels for classifying the images’ rotations to improve GAN performance. We emphasize all three GANs experimented are

unconditional, meaning they do not require conditioning on labeled data.

For clarity, we highlight here that InfoMax-GAN is equivalent to SNGAN with our proposed objective, and SSGAN is equivalent to SNGAN with the rotation task objective. We show that InfoMax-GAN *alone* is able to achieve highly competitive performance and significant improvements over SSGAN. We detail the exact architectures used for all models and datasets in Appendix C.

B. Experimental Settings

a) Datasets: We evaluate our models across five different datasets: ImageNet [34], CelebA [35], CIFAR-10 [36], STL-10 [37], and CIFAR-100 [36]. For preprocessing our images, we follow settings in [12], [30]. For ImageNet, we use the 1.3M training images downsampled to size 128×128 . For CelebA, we use the aligned version of the 200K images downsampled to size 128×128 . For CIFAR-10 and CIFAR-100 we use all 50K training images, and for STL-10, we use all 100K unlabeled images downsampled to size 48×48 .

b) Training: For all models, we use Residual Network [38] backbones following [29]. For all datasets, we adopt the Adam optimizer [39] with a learning rate of 2×10^{-4} and batch size of 64, following [3], [29]. For CIFAR-10, CIFAR-100 and STL-10, we follow settings in [30] by linearly decaying learning rate over 100K generator steps, each taken every 5 discriminator update steps. For ImageNet, we follow [29] by increasing the number of generator updates to 450K steps instead, but with no learning rate decay. For CelebA, we follow [12] by taking 100K generator steps, each taken after 2 discriminator updates and with no learning rate decay.

For all models and datasets, we set $\alpha = \beta = 0.2$, to balance the contrastive loss to be on the same scale as the GAN loss

initially. This scaling principle is similar to what is applied in [40], with details left to our ablation study. We further perform ablation studies for α and β to show our framework is robust to changes in these hyperparameters. Finally, for fairness in our comparisons, we re-implemented all considered models using the same code base and framework, and conducted all experiments under the *same training conditions*.

c) *Evaluation*: To assess the quality of generated images, we employ three different metrics: Fréchet Inception Distance (FID) [7], Kernel Inception Distance (KID) [41], and Inception Score (IS) [8]. Firstly, FID is a popular metric measuring the diversity of generated images, which we adopt for ease of comparisons since it is widely used in the literature. Formally, FID computes the Wasserstein-2 Distance between features produced by a pre-trained Inception [42] network for input real and generated images, and is defined as:

$$d_{\text{FID}} = \|\mu_r - \mu_g\|_2^2 + \text{Tr}(\Sigma_r + \Sigma_g - 2(\Sigma_r \Sigma_g)^{\frac{1}{2}}) \quad (11)$$

where μ_r and Σ_r denotes the mean and covariance of feature vectors produced by forwarding real images through a pre-trained Inception [42] network, and μ_g and Σ_g similarly represents the equivalent for fake images. Intuitively, FID measures the diversity of the generated images, since the features of the generated images should ideally have a small distance with those of real images if they look similar on average. However, we note that FID can produce highly biased estimates [41], where using larger sample sizes can produce better scores, which can causes FID comparisons to be often mismatched [43] in practice. Thus, we emphasize for fairness in comparisons, we use the *exact* same number of real and fake images for computing FID.

KID is an alternative metric highly correlated with FID that also measures diversity of images, but produces unbiased estimates [41], which is useful for corroborating our findings on FID. Formally, KID measures the square of the Maximum Mean Discrepancy (MMD) [44] between two probability distributions in a metric space, and can be defined as:

$$\begin{aligned} d_{\text{KID}} &= \text{MMD}^2(X, Y) \\ &= \frac{1}{m(m-1)} \sum_{i \neq j}^m k(x_i, x_j) \\ &\quad + \frac{1}{n(n-1)} \sum_{i \neq j}^n k(y_i, y_j) - \frac{2}{mn} \sum_{i=1}^m \sum_{j=1}^n k(x_i, y_j) \end{aligned} \quad (12)$$

for two random variables X and Y from different distributions, sample sizes m and n , and k is the polynomial kernel defined as:

$$k(x, y) = \left(\frac{1}{d} x^T y + 1\right)^3 \quad (13)$$

where d represents the dimensions of the samples. Intuitively, MMD measures the distance between distributions using a function from a class of witness functions such that if the true distance between the distributions is zero, the distance between the mean embeddings produced by this function will also be zero. Here, the polynomial kernel is cubic in order to measure the first three moments of the distributions (mean, variance, and skewness), and the embedding is defined on the feature

space through the Inception network. Similar to FID, we use the same number of real and fake images for all models when computing KID.

Finally, IS aims to measure the realism of generated images using the same Inception network, and can be formally defined as:

$$d_{\text{IS}} = \exp(\mathbb{E}_{x \sim p_g} \mathcal{D}_{\text{KL}}(p(y|x) || p(y))) \quad (14)$$

where a high score is achieved if the conditional class distribution $p(y|x)$ has low entropy and the marginal class distribution $p(y)$ has high entropy, causing a large KL divergence between the two distributions for some samples x from the generated image distribution p_g . Intuitively, a large score is produced if the Inception network gives a high probability to one class, indicating it looks realistically in one class. Thus, IS tends to correlate well with human assessment for quality of images [8].

In this paper, we compute all scores using 3 different random seeds to report the mean and standard deviation. We emphasize that all evaluation conditions are kept the same for all models, in order to ensure the accuracy and fairness in our comparisons. Exact details on the sample sizes used for all metrics can be found at Appendix A-A.

C. Results

a) *Improved image synthesis*: On FID, as seen in Table I, InfoMax-GAN achieves a consistent and significant improvement in FID across all datasets over the baseline SNGAN, and significantly so over SSGAN on multiple datasets. On the challenging high resolution ImageNet dataset, InfoMax-GAN improves by **6.8 points** over SNGAN, and **3.6 points** over SSGAN. On the high resolution CelebA, while SSGAN could not improve over the baseline SNGAN, as similarly noted in [12], InfoMax-GAN improves by **3.4 points** over SNGAN, and **5.8 points** over SSGAN. This suggests our approach is versatile and can generalise across multiple data domains.

On STL-10, InfoMax-GAN achieves an improvement of **3.0 points** over SNGAN and **1.5 points** over SSGAN. Interestingly, while InfoMax-GAN performs similarly as SSGAN on CIFAR-10 with around **0.5 points** difference, it is able to achieve **3.4 points** improvements on CIFAR-100 when the number of classes increase. We conjecture this is due to the tendency for SSGAN to generate images that are easy to rotate [45], which sacrifices diversity and reduces FID when there are more classes. This observation also supports InfoMax-GAN's larger improvements on ImageNet, which has 1000 classes. Here, we emphasize that due to FID's biased nature, *lower* FID scores can in fact be achieved for all datasets if we increase the sample size for computing FID [41], without changing the model at all. However, our experiments show that the margin of improvements between models remain the same even with larger sample sizes above our current configuration, thus removing the need to use larger sample sizes.

Similarly, for alternative metrics like KID and IS, InfoMax-GAN achieves a highly competitive performance and improves over the state-of-the-art works. On IS, InfoMax-GAN is able to improve from **0.2 to 0.4 points** over SSGAN for all datasets except CIFAR-10, where the margin is less than **0.1 points** and

Metric	Dataset	Resolution	Models		
			SNGAN	SSGAN	InfoMax-GAN
FID	ImageNet	128 × 128	65.74 ± 0.31	62.48 ± 0.31	58.91 ± 0.14
	CelebA	128 × 128	14.04 ± 0.02	16.39 ± 0.09	10.63 ± 0.04
	STL-10	48 × 48	40.48 ± 0.07	38.97 ± 0.23	37.49 ± 0.05
	CIFAR-100	32 × 32	24.76 ± 0.16	24.64 ± 0.16	21.22 ± 0.26
	CIFAR-10	32 × 32	18.63 ± 0.22	16.59 ± 0.13	17.14 ± 0.20
KID	ImageNet	128 × 128	0.0663 ± 0.0004	0.0616 ± 0.0004	0.0579 ± 0.0004
	CelebA	128 × 128	0.0076 ± 0.0001	0.0101 ± 0.0001	0.0063 ± 0.0001
	STL-10	48 × 48	0.0369 ± 0.0002	0.0332 ± 0.0004	0.0326 ± 0.0002
	CIFAR-100	32 × 32	0.0156 ± 0.0003	0.0161 ± 0.0002	0.0135 ± 0.0004
	CIFAR-10	32 × 32	0.0125 ± 0.0001	0.0101 ± 0.0002	0.0112 ± 0.0001
IS	ImageNet	128 × 128	13.05 ± 0.05	13.30 ± 0.03	13.68 ± 0.06
	CelebA	128 × 128	2.72 ± 0.01	2.63 ± 0.01	2.84 ± 0.01
	STL-10	48 × 48	8.04 ± 0.07	8.25 ± 0.06	8.54 ± 0.12
	CIFAR-100	32 × 32	7.57 ± 0.11	7.56 ± 0.07	7.86 ± 0.10
	CIFAR-10	32 × 32	7.97 ± 0.06	8.17 ± 0.06	8.08 ± 0.08

TABLE I: Mean FID, KID and IS scores of all models across different datasets, computed across 3 different seeds. FID and KID: lower is better. IS: higher is better.

Dataset	Resolution	Models	
		SSGAN	SSGAN + IM
ImageNet	128 × 128	62.48 ± 0.31	56.45 ± 0.29
CelebA	128 × 128	16.39 ± 0.09	11.93 ± 0.14
STL-10	48 × 48	38.97 ± 0.23	37.73 ± 0.06
CIFAR-100	32 × 32	24.64 ± 0.16	21.40 ± 0.20
CIFAR-10	32 × 32	16.59 ± 0.13	15.42 ± 0.08

TABLE II: Mean FID scores (lower is better) of SSGAN before and after applying our method: “+ IM” refers to adding our proposed InfoMax-GAN objective. Our improvement is orthogonal to that of SSGAN and can be easily integrated into existing frameworks.

within the standard deviation, indicating a similar performance. Similar to its FID performance on CelebA, SSGAN also performs worse in terms of IS compared to the baseline SNGAN, suggesting its failure mode on faces is not just due to a limited diversity, but also due to poorer quality. In contrast, InfoMax-GAN is able to improve on IS over SNGAN and SSGAN significantly. Finally, on KID, we confirm our result on FID: where FID is better, KID is also better. This further substantiates our FID results and the fact that InfoMax-GAN is able to generate more diverse images across these datasets, with no obvious failure modes unlike in SSGAN.

b) Orthogonal improvements: We show that our improvements are orthogonal to those in SSGAN in Table II: when incorporating our objective into SSGAN, FID is improved across all datasets significantly, achieving even larger improvements of approximately **2.5 points** for the challenging ImageNet dataset. Thus, our method is flexible and can be easily integrated into existing state-of-the-art frameworks like SSGAN.

c) Improved training stability: Similar to [12], we test training stability through evaluating the sensitivity of model performance when hyperparameters are varied across a range of popular settings for training GANs, such as the Adam parameters (β_1, β_2) and number of discriminator steps per

generator step, n_{dis} . These sets of hyperparameters are based on settings in [3], [12], [29], [46], [47], which are well-tested settings used in popular works such as SNGAN and WGAN-GP [3]. As seen in Table III, in comparison to SNGAN at the *same architectural capacity*, InfoMax-GAN obtains a consistent FID improvement for different datasets even in instances where GAN training does not converge (e.g. when $n_{\text{dis}} = 1$). The variability in FID scores for the InfoMax-GAN is much lower than SSGAN, showing its robustness to changes in training hyperparameters. Finally, we observe while different sets of (β_1, β_2) work better for each dataset, our method is able to stabilize training and obtain significant improvements in all these settings, *without any hyperparameter tuning*. This can be useful in practice when training new GANs or on novel datasets, where training can be highly unstable when other hyperparameters are not well-tuned.

In Figure 4, we show that our method greatly stabilises GAN training to achieve a faster convergence of GAN training early on, with a consistent improvement throughout the training process. We attribute this to the fact that under an additional constraint where the global features of images are constrained to have high mutual information with all their local features [22], the space of generated data distribution p_g is also constrained, thereby causing p_g to change less radically and ultimately stabilising the GAN training environment.

d) Low computational cost: In practice, our method takes only a fraction of the training time. Similar to [29], we show this by profiling the training time for 100 generator update steps. From Figure 5, we see our approach takes up minimal time at less than 0.1% of training time per update, across all n_{dis} for both CIFAR-10 and STL-10. This is because in practice, we only need 2 shallow (1 hidden layer) MLP networks to compute the contrastive loss. Furthermore, from Table III, we note that at $n_{\text{dis}} = 2$, InfoMax-GAN has a consistently better FID than SNGAN at $n_{\text{dis}} = 5$ at approximately *half the training time*, since a large n_{dis} is a significant bottleneck in training time. Thus, our approach is practical for training GANs with less time taken, and with minimal computational overhead,

β_1	β_2	n_{dis}	CIFAR-10		STL-10	
			SNGAN	InfoMax-GAN	SNGAN	InfoMax-GAN
0.0	0.9	1	164.74 \pm 0.42	24.42 \pm 0.18	267.10 \pm 0.20	54.29 \pm 0.13
0.0	0.9	2	20.87 \pm 0.19	18.08 \pm 0.27	46.65 \pm 0.18	38.96 \pm 0.31
0.0	0.9	5	18.63 \pm 0.22	17.14 \pm 0.20	40.48 \pm 0.07	37.49 \pm 0.05
0.5	0.999	1	73.07 \pm 0.20	20.58 \pm 0.10	134.51 \pm 0.37	62.28 \pm 0.07
0.5	0.999	2	18.74 \pm 0.24	17.19 \pm 0.32	40.67 \pm 0.29	40.54 \pm 0.20
0.5	0.999	5	21.10 \pm 0.89	18.39 \pm 0.04	84.20 \pm 0.67	75.72 \pm 0.19

TABLE III: Mean FID scores (lower is better) across a range of hyperparameter settings. (β_1, β_2) represents the hyperparameters of the Adam optimizer, and n_{dis} represents the number of discriminator steps per generator step. Our method performs robustly in a wide range of training settings *without any tuning*.

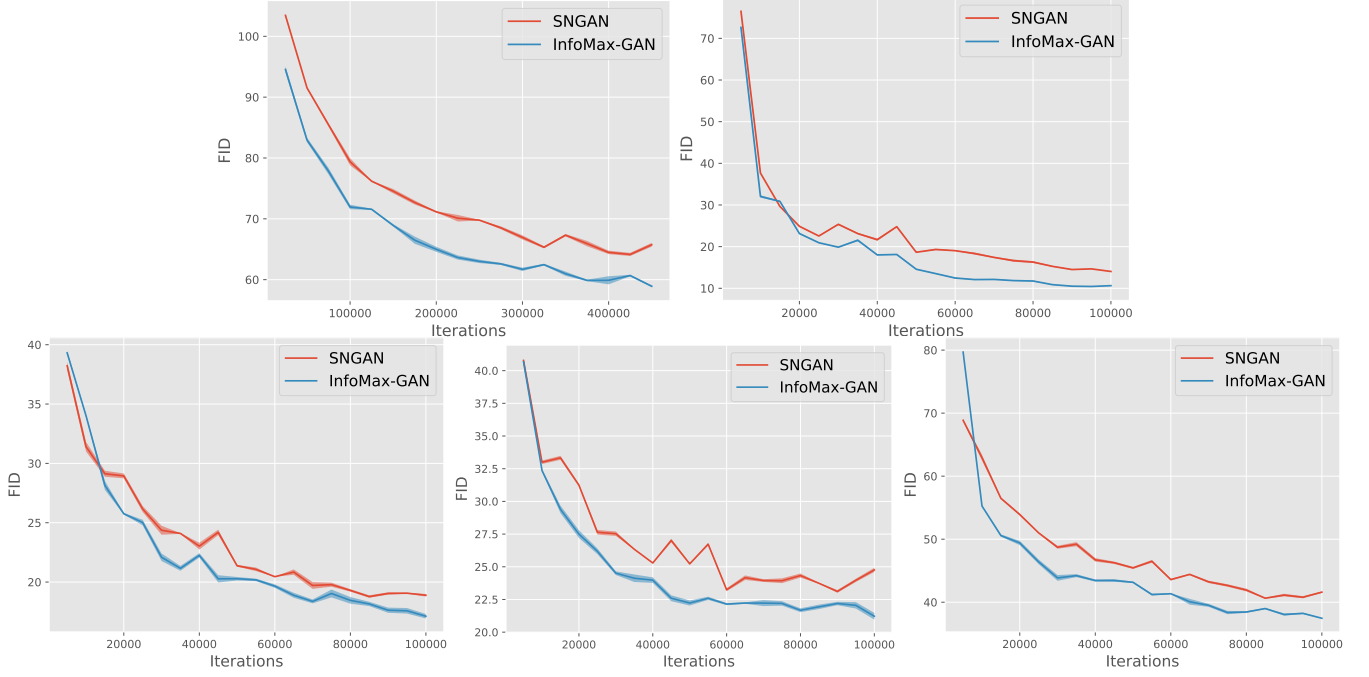


Fig. 4: Our approach stabilises GAN training significantly to achieve a faster convergence and consistent improvement in FID for all models across all datasets. Top row: ImageNet, CelebA. Bottom row: CIFAR-10, CIFAR-100, STL-10.

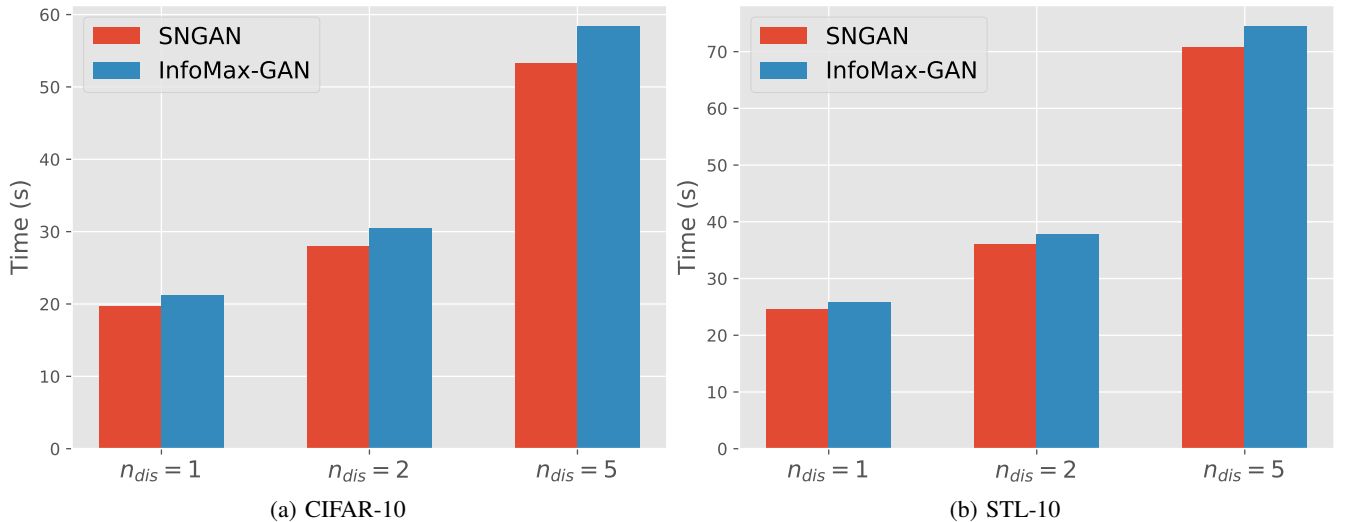


Fig. 5: Training time for 100 generator update steps across different n_{dis} values for CIFAR-10 and STL-10, as computed using the same hardware. In general, our proposed framework incurs significantly less time than the overall training cost.

Metric	K	DCGAN	DCGAN + IM
# Modes	1/4	27.67 \pm 0.47	62.00 \pm 1.63
# Modes	1/2	610.00 \pm 8.83	716.67 \pm 1.25
$\mathcal{D}_{\text{KL}}(p q)$	1/4	5.44 \pm 0.01	4.68 \pm 0.01
$\mathcal{D}_{\text{KL}}(p q)$	1/2	1.98 \pm 0.01	1.64 \pm 0.01

TABLE IV: Number of modes (higher is better) recovered by the generator on the Stacked MNIST dataset, where the maximum value is 1000; and KL divergence $\mathcal{D}_{\text{KL}}(p||q)$ between the distribution of generated modes p and the uniform distribution q , where lower is better. ‘+ IM’ refers to adding our proposed InfoMax-GAN objective.

our method can be easily integrated into existing frameworks without becoming a bottleneck.

e) Improved mode recovery: Following settings in [48], we re-implement the DCGAN [47] in [48] and evaluate its ability in recovering all 1000 modes of the Stacked MNIST dataset [48], composed by randomly stacking 3 grayscale MNIST [49] digits into an RGB image, resulting in 1000 possible modes. We use a pre-trained MNIST classifier to classify each color channel of a generated image, and the model is said to recover 1 mode if it generates at least 1 image for that mode. We similarly set $K \in \{\frac{1}{4}, \frac{1}{2}\}$, where K indicates the size of the discriminator relative to the generator. Intuitively, the smaller K is, the easier it is for the generator to fool the discriminator with just a few modes, resulting in less modes recovered. Furthermore, we compute the KL divergence $\mathcal{D}_{\text{KL}}(p||q)$ between the generated mode distribution p and optimal uniform distribution of the modes q . We see from Table IV that our method helps to recover more modes for all K , with the recovered distribution having a consistently lower KL divergence with the ideal uniform distribution as a result.

f) Qualitative comparisons: In Figure 6, we show generated images at 128×128 resolution for CelebA. In general, we observe that images generated by InfoMax-GAN is able to have less visual artifacts for both the background and facial attributes, with even attributes like spectacles and caps generated. In contrast, both SNGAN and SSGAN generated images tend to have more severe background artifacts, with certain prominent facial features like eyes and noses not well blended together. This blending problem is more commonly seen in SSGAN generated images, which may explain its worse FID performance compared to both SNGAN and InfoMax-GAN. We further provide image samples randomly generated for all datasets in Appendix A-B.

D. Ablation Studies

a) RKHS dimensions: As seen in Table V, our proposed framework is robust to the choice of R , with the FID remaining consistent in their range of values. We attribute this to the fact that the InfoMax critics are simple MLP networks with only 1 hidden layer, which is sufficient for achieving good representations in practice [17]. We note for all our experiments in Tables I, II, and III, we used $R = 1024$.

R	Relative Size	FID Score
256	2	17.07 \pm 0.25
512	4	17.21 \pm 0.15
1024	8	17.14 \pm 0.20
2048	16	17.80 \pm 0.05
4096	32	17.38 \pm 0.11

TABLE V: Mean FID scores (lower is better) for InfoMax-GAN on CIFAR-10 when the RKHS dimension R is varied. Relative size here refers to how much larger R is relative to the discriminator feature map depth of 128, in terms of multiplicative factor.

b) Sensitivity of α and β hyperparameters: In Figure 7a, we performed a large sweep of α and β from 0.0 to 1.0, and see that $\alpha = \beta = 0.2$ obtains the best performance for our method. From Figure 7b, we observe our InfoMax objective for the discriminator is important for improving GAN performance: as β is decreased, keeping $\alpha = 0.2$, FID deteriorates. Interestingly, we observe when $\alpha = 0$ and $\beta = 0.2$, having the InfoMax objective for the discriminator alone is sufficient in gaining FID improvements. This confirms our intuition of the role of information maximization in mitigating discriminator catastrophic forgetting to stabilize the GAN training environment and improve FID. However, the performance improves when the generator is also trained on the InfoMax objective, at $\alpha \in \{0.1, 0.2\}$ and $\beta = 0.2$, which affirms our prior intuition that the contrastive nature of the objective helps the generator reduce mode collapse and improve FID. We note that apart from this ablation study, we used $\alpha = \beta = 0.2$ for all experiments reported in this paper.

c) Relative Scale of Objective: From Figure 8, we see in both our chosen hyperparameters of $\alpha = \beta = 0.2$ and the other extreme of $\alpha = \beta = 1.0$, the InfoMax objective loss decays very quickly relative to the GAN loss. In practice, we found that $\alpha = \beta = 0.2$ performs better, which could be attributed to the relative magnitude of the InfoMax objective loss at the start of the training. When $\alpha = \beta = 0.2$, the scales of the GAN and InfoMax objective losses are approximately equal initially. We highlight this is the same loss scaling principle applied in [40].

d) Position of feature maps: While we have chosen the local and global features to be the penultimate and final features of the discriminator encoder respectively, we examine the effect of alternative designs. For clarity, we note there is only *one* global feature vector, which is the final feature output of the encoder. Correspondingly, our design can be called local-global, and other designs involving extracting intermediate local feature maps $C_{\psi,k}(x), 1 \leq k \leq n$ can be described as local-local. However, in practice, our original design of local-global is the only feasible option compared to local-local option, mainly due to the memory consumption: for any two feature maps of spatial size $M_1 \times M_1$ and $M_2 \times M_2$ respectively, we have the space complexity as $O(NM_1^2M_2^2R)$ for batch size N and RKHS R . Fixing the first feature map size, the local-local approach has space complexity growing quadratically on the second feature map size M_2 , which is in turn dependent on the image resolution. On the other hand, the local-global approach



Fig. 6: Generated CelebA images at 128×128 resolution for (a) SNGAN, (b) SSGAN, and (c) InfoMax-GAN. In general, we observe InfoMax-GAN generated images have less visual artifacts in both the background and the facial attributes. We note these images are randomly generated and non-cherry picked.

effectively sets $M_2 = 1$, which dramatically reduces memory consumption.

In fact, in practice, we found the local-local approach cannot scale to datasets above 32×32 resolution as it would exceed 11GB for a single GPU. To still test this approach on the 32×32 resolution CIFAR-10 dataset, we reduce the memory consumption by randomly sampling only half of local

spatial vectors from each feature map. Even so, the memory consumption is approximately 7 times of the local-global approach, making it highly memory intensive. In contrast, the local-global approach scales for even high resolution (e.g. 128×128) datasets and takes only a small portion of the memory size compared to the GAN models. Importantly, the local-local approach worsens FID by **3.1 points** from

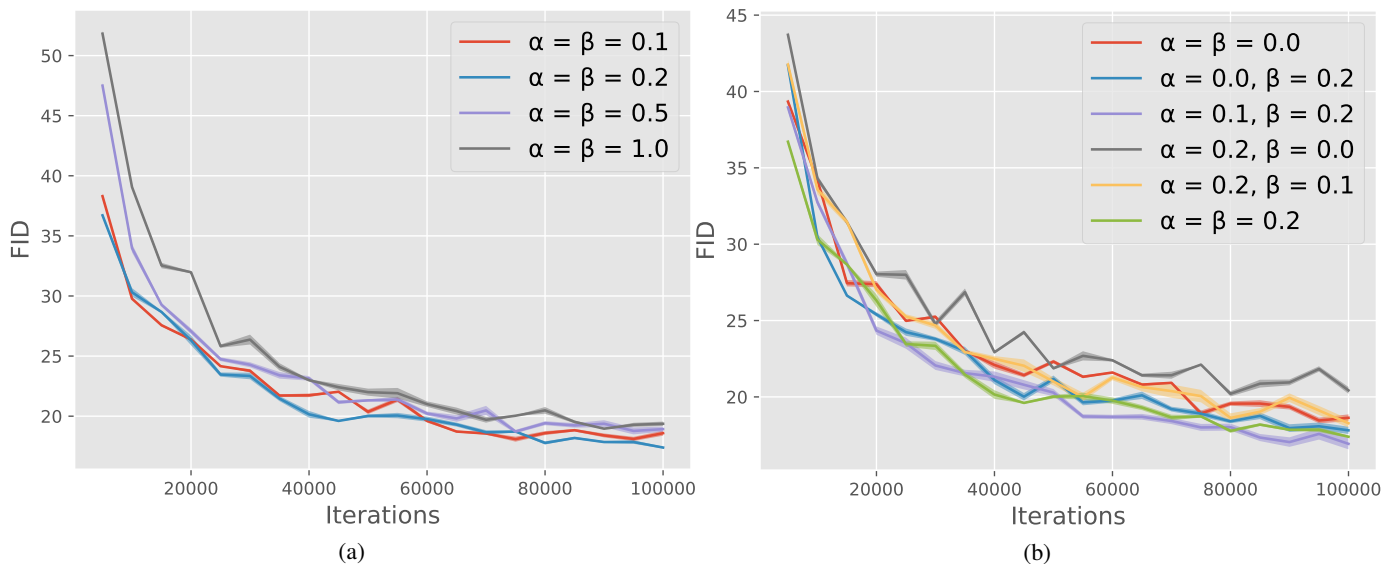


Fig. 7: (a) CIFAR-10 FID curves for InfoMax-GAN across a large sweep of α and β hyperparameters, showing $\alpha = \beta = 0.2$ performs the best. However, the overall performance remains approximately similar. (b) We perform a small sweep around the chosen hyperparameters $\alpha = \beta = 0.2$.

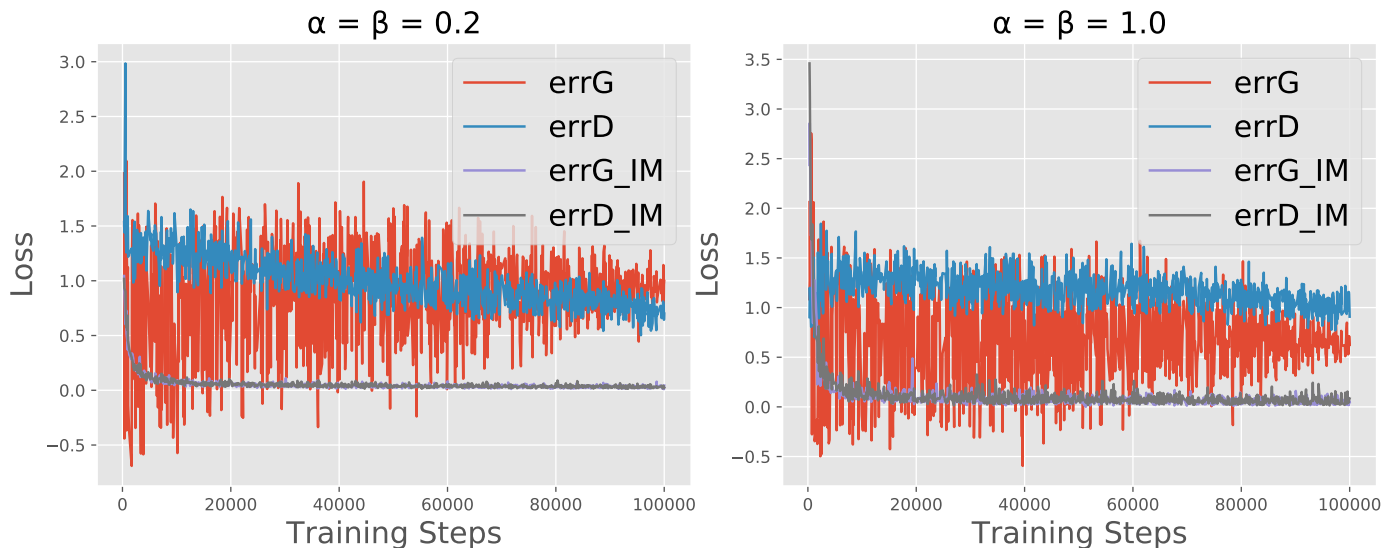


Fig. 8: We show that the InfoMax objective loss decays very quickly regardless of the choice of scale for both α and β . errD and errG represents the GAN losses for the discriminator and generator respectively, and similarly, errD_IM and errG_IM represents the InfoMax objective losses for the discriminator and generator respectively.

17.14 ± 0.20 to 20.20 ± 0.05 . Thus, this ablation study show that in practice, our current design is the most optimal for achieving both performance and memory consumption gains.

e) Effect of spectral normalizing critic: Interestingly, using spectral normalisation for the InfoMax-GAN critic networks leads to FID improvements. On CIFAR-10, using spectral normalisation for these critic networks improved FID by **1.5 points** from 18.67 ± 0.25 to 17.14 ± 0.20 . We conjecture this could be related to the Wasserstein Dependency Measure [50], a variant of mutual information which replaces the KL divergence term with Wasserstein distance, as measured using encoders from the class of 1-Lipschitz functions. However, in contrast to this work, our method enforces 1-Lipschitzness of

the encoder using spectral normalization rather than gradient penalty. A theoretical treatment of this relationship is beyond the scope of this paper, which we leave as future work.

V. RELATED WORK

a) Mode collapse and catastrophic forgetting: Early works in reducing mode collapse include Unrolled GAN [48], which restructures the generator objective with respect to unrolled discriminator optimization updates. These works often focused on assessing the number of modes recovered by a GAN based on synthetic datasets [48], [51], [52]. Subsequent works include MSGAN [53], which introduces a regularization encouraging conditional GANs to seek out minor modes often

missed when training. These works instead focus on direct metrics [7], [8], [41], [54]–[56] for assessing the diversity and quality of generated images. In our work, we utilized both types of metrics for assessment. Previous approaches to mitigate catastrophic forgetting in GANs include using forms of memory [8], [57], [58], such as checkpoint averaging. [12] demonstrates the mitigation of catastrophic forgetting using a representation learning approach, which we built upon.

b) Representation learning and GANs: To the best of our knowledge, the closest work in *methodology* to ours is the state-of-the-art SSGAN, which demonstrates the use of a representation learning approach of predicting rotations [59] to mitigate GAN forgetting and hence improve GAN performance. In contrast to SSGAN, our work uses a contrastive learning and information maximization task instead, which we demonstrate to simultaneously mitigate *both* GAN forgetting and mode collapse. Furthermore, our work is able to overcome failure modes demonstrated in SSGAN, such as in datasets involving faces [12]. For fair and accurate comparisons, our work compared with SSGAN using the *exact* same architectural capacity, training and evaluation settings.

c) Information theory and GANs: The most prominent work in utilizing mutual information maximization for GANs is InfoGAN, but we emphasize here that our work has a *different focus*: while InfoGAN focuses on learning disentangled representations, our goal is to improve image synthesis. For clarity, we illustrate the specific differences with InfoGAN in Appendix B. Other approaches employing information theoretic principles include Variational GAN (VGAN) [60], which uses an information bottleneck [61] to regularize the discriminator representations; with [62]–[64] extending to minimise divergences apart from the original JS divergence. In contrast to these works, our work employs the InfoMax principle to improve discriminator learning, and provides a clear connection to how this improves GAN training via the mitigation of catastrophic forgetting.

VI. CONCLUSION AND FUTURE WORK

In this paper, we presented the InfoMax-GAN framework for improving natural image synthesis through simultaneously alleviating two key issues in GANs: catastrophic forgetting of the discriminator (via information maximization), and mode collapse of the generator (via contrastive learning). Our approach significantly improves on the natural image synthesis task for *five* widely used datasets, and further overcome failure modes in state-of-the-art models like SSGAN. Our approach is simple and practical: it has only one auxiliary objective, performs robustly in a wide range of training settings without any hyperparameter tuning, has low computational cost, and demonstrated improvements even when integrated to existing state-of-the-art models like SSGAN. As future work, it would be interesting to explore this framework for different tasks, such as in 3D view synthesis, where one could formulate objectives involving mutual information and adjacent views.

To the best of our knowledge, our work is the first to investigate using information maximization and contrastive learning to improve GAN image synthesis performance, and we hope our work opens up new possibilities in this direction.

ACKNOWLEDGEMENTS

The authors thank Ting Chen for the helpful discussions and information on running the catastrophic forgetting experiment.

REFERENCES

- [1] I. Goodfellow, J. Pouget-Abadie, M. Mirza, B. Xu, D. Warde-Farley, S. Ozair, A. Courville, and Y. Bengio, “Generative Adversarial Nets,” in *Advances in Neural Information Processing Systems*, 2014, pp. 2672–2680.
- [2] A. Odena, “Open Questions About Generative Adversarial Networks,” *Distill*, 2019, <https://distill.pub/2019/gan-open-problems>.
- [3] I. Gulrajani, F. Ahmed, M. Arjovsky, V. Dumoulin, and A. C. Courville, “Improved Training of Wasserstein Gans,” in *Advances in Neural Information Processing Systems*, 2017, pp. 5767–5777.
- [4] A. Odena, C. Olah, and J. Shlens, “Conditional Image Synthesis with Auxiliary Classifier Gans,” in *Proceedings of the 34th International Conference on Machine Learning-Volume 70*. JMLR. org, 2017, pp. 2642–2651.
- [5] N.-T. Tran, T.-A. Bui, and N.-M. Cheung, “Improving GAN with Neighbors Embedding and Gradient Matching,” in *Proceedings of the AAAI Conference on Artificial Intelligence*, vol. 33, 2019, pp. 5191–5198.
- [6] —, “Dist-Gan: An Improved GAN Using Distance Constraints,” in *The European Conference on Computer Vision (ECCV)*, September 2018.
- [7] M. Heusel, H. Ramsauer, T. Unterthiner, B. Nessler, and S. Hochreiter, “Gans Trained by a Two Time-Scale Update Rule Converge to a Local Nash Equilibrium,” in *Advances in Neural Information Processing Systems*, 2017, pp. 6626–6637.
- [8] T. Salimans, I. Goodfellow, W. Zaremba, V. Cheung, A. Radford, and X. Chen, “Improved Techniques for Training Gans,” in *Advances in Neural Information Processing Systems*, 2016, pp. 2234–2242.
- [9] I. Goodfellow, “NIPS 2016 Tutorial: Generative Adversarial Networks,” *arXiv Preprint arXiv:1701.00160*, 2016.
- [10] N.-T. Tran, V.-H. Tran, N.-B. Nguyen, and N.-M. Cheung, “An Improved Self-supervised GAN via Adversarial Training,” *arXiv preprint arXiv:1905.05469*, 2019.
- [11] M. McCloskey and N. J. Cohen, “Catastrophic Interference in Connectionist Networks: The Sequential Learning Problem,” in *Psychology of Learning and Motivation*. Elsevier, 1989, vol. 24, pp. 109–165.
- [12] T. Chen, X. Zhai, M. Ritter, M. Lucic, and N. Houlsby, “Self-Supervised Gans via Auxiliary Rotation Loss,” in *Proceedings of the IEEE Conference on Computer Vision and Pattern Recognition*, 2019, pp. 12 154–12 163.
- [13] J. Kirkpatrick, R. Pascanu, N. Rabinowitz, J. Veness, G. Desjardins, A. A. Rusu, K. Milan, J. Quan, T. Ramalho, A. Grabska-Barwinska et al., “Overcoming Catastrophic Forgetting in Neural Networks,” *Proceedings of the National Academy of Sciences*, vol. 114, no. 13, pp. 3521–3526, 2017.
- [14] R. Kemker, M. McClure, A. Abitino, T. L. Hayes, and C. Kanan, “Measuring Catastrophic Forgetting in Neural Networks,” in *Thirty-Second AAAI Conference on Artificial Intelligence*, 2018.
- [15] Y. Bengio, A. Courville, and P. Vincent, “Representation Learning: A Review and New Perspectives,” *IEEE Transactions on Pattern Analysis and Machine Intelligence*, vol. 35, no. 8, pp. 1798–1828, 2013.
- [16] R. Linsker, “Self-Organization in a Perceptual Network,” *Computer*, vol. 21, no. 3, pp. 105–117, 1988.
- [17] M. Tschannen, J. Djolonga, P. K. Rubenstein, S. Gelly, and M. Lucic, “On Mutual Information Maximization for Representation Learning,” *arXiv Preprint arXiv:1907.13625*, 2019.
- [18] B. Poole, S. Ozair, A. van den Oord, A. A. Alemi, and G. Tucker, “On Variational Lower Bounds of Mutual Information,” in *NeurIPS Workshop on Bayesian Deep Learning*, 2018.
- [19] P. Bachman, R. D. Hjelm, and W. Buchwalter, “Learning Representations by Maximizing Mutual Information Across Views,” *arXiv Preprint arXiv:1906.00910*, 2019.
- [20] Y. Tian, D. Krishnan, and P. Isola, “Contrastive Multiview Coding,” *arXiv Preprint arXiv:1906.05849*, 2019.
- [21] A. v. d. Oord, Y. Li, and O. Vinyals, “Representation Learning with Contrastive Predictive Coding,” *arXiv Preprint arXiv:1807.03748*, 2018.
- [22] R. D. Hjelm, A. Fedorov, S. Lavoie-Marchildon, K. Grewal, P. Bachman, A. Trischler, and Y. Bengio, “Learning Deep Representations by Mutual Information Estimation and Maximization,” *arXiv Preprint arXiv:1808.06670*, 2018.
- [23] O. J. Hénaff, A. Razavi, C. Doersch, S. Eslami, and A. v. d. Oord, “Data-Efficient Image Recognition with Contrastive Predictive Coding,” *arXiv Preprint arXiv:1905.09272*, 2019.

- [24] S. Löwe, P. O'Connor, and B. S. Veeling, "Greedy InfoMax for Biologically Plausible Self-Supervised Representation Learning," *arXiv Preprint arXiv:1905.11786*, 2019.
- [25] L. Kong, C. d. M. d'Autume, W. Ling, L. Yu, Z. Dai, and D. Yogatama, "A Mutual Information Maximization Perspective of Language Representation Learning," *arXiv Preprint arXiv:1910.08350*, 2019.
- [26] L. Paninski, "Estimation of Entropy and Mutual Information," *Neural Computation*, vol. 15, no. 6, pp. 1191–1253, 2003.
- [27] T. Chen, S. Kornblith, M. Norouzi, and G. Hinton, "A Simple Framework for Contrastive Learning of Visual Representations," *arXiv Preprint arXiv:2002.05709*, 2020.
- [28] N. Aronszajn, "Theory of Reproducing Kernels," *Transactions of the American Mathematical Society*, vol. 68, no. 3, pp. 337–404, 1950.
- [29] T. Miyato, T. Kataoka, M. Koyama, and Y. Yoshida, "Spectral Normalization for Generative Adversarial Networks," *arXiv Preprint arXiv:1802.05957*, 2018.
- [30] T. Miyato and M. Koyama, "cGANs with Projection Discriminator," *arXiv Preprint arXiv:1802.05637*, 2018.
- [31] H. Zhang, I. Goodfellow, D. Metaxas, and A. Odena, "Self-Attention Generative Adversarial Networks," in *International Conference on Machine Learning*, 2019, pp. 7354–7363.
- [32] A. Brock, J. Donahue, and K. Simonyan, "Large Scale Gan Training for High Fidelity Natural Image Synthesis," *arXiv Preprint arXiv:1809.11096*, 2018.
- [33] X. Gong, S. Chang, Y. Jiang, and Z. Wang, "AutoGAN: Neural Architecture Search for Generative Adversarial Networks," *arXiv Preprint arXiv:1908.03835*, 2019.
- [34] J. Deng, W. Dong, R. Socher, L.-J. Li, K. Li, and L. Fei-Fei, "Imagenet: A Large-Scale Hierarchical Image Database," in *2009 IEEE Conference on Computer Vision and Pattern Recognition*. Ieee, 2009, pp. 248–255.
- [35] Z. Liu, P. Luo, X. Wang, and X. Tang, "Deep Learning Face Attributes in the Wild," in *Proceedings of International Conference on Computer Vision (ICCV)*, December 2015.
- [36] A. Krizhevsky, G. Hinton *et al.*, "Learning Multiple Layers of Features from Tiny Images," Citeseer, Tech. Rep., 2009.
- [37] A. Coates, A. Ng, and H. Lee, "An Analysis of Single-Layer Networks in Unsupervised Feature Learning," in *Proceedings of the Fourteenth International Conference on Artificial Intelligence and Statistics*, 2011, pp. 215–223.
- [38] K. He, X. Zhang, S. Ren, and J. Sun, "Deep Residual Learning for Image Recognition," in *Proceedings of the IEEE Conference on Computer Vision and Pattern Recognition*, 2016, pp. 770–778.
- [39] D. P. Kingma and J. Ba, "Adam: A Method for Stochastic Optimization," *arXiv Preprint arXiv:1412.6980*, 2014.
- [40] X. Chen, Y. Duan, R. Houthoofd, J. Schulman, I. Sutskever, and P. Abbeel, "Infogan: Interpretable Representation Learning by Information Maximizing Generative Adversarial Nets," in *Advances in Neural Information Processing Systems*, 2016, pp. 2172–2180.
- [41] M. Bińkowski, D. J. Sutherland, M. Arbel, and A. Gretton, "Demystifying Mmd Gans," *arXiv Preprint arXiv:1801.01401*, 2018.
- [42] C. Szegedy, V. Vanhoucke, S. Ioffe, J. Shlens, and Z. Wojna, "Rethinking the Inception Architecture for Computer Vision," in *Proceedings of the IEEE Conference on Computer Vision and Pattern Recognition*, 2016, pp. 2818–2826.
- [43] K. Kurach, M. Lučić, X. Zhai, M. Michalski, and S. Gelly, "A Large-scale Study on Regularization and Normalization in GANs," in *International Conference on Machine Learning*, 2019, pp. 3581–3590.
- [44] A. Gretton, K. M. Borgwardt, M. J. Rasch, B. Schölkopf, and A. Smola, "A Kernel Two-Sample Test," *Journal of Machine Learning Research*, vol. 13, no. Mar, pp. 723–773, 2012.
- [45] N.-T. Tran, V.-H. Tran, B.-N. Nguyen, L. Yang *et al.*, "Self-Supervised GAN: Analysis and Improvement with Multi-Class Minimax Game," in *Advances in Neural Information Processing Systems*, 2019, pp. 13 232–13 243.
- [46] D. Warde-Farley and Y. Bengio, "Improving Generative Adversarial Networks with Denoising Feature Matching," 2016.
- [47] A. Radford, L. Metz, and S. Chintala, "Unsupervised Representation Learning with Deep Convolutional Generative Adversarial Networks," *arXiv Preprint arXiv:1511.06434*, 2015.
- [48] L. Metz, B. Poole, D. Pfau, and J. Sohl-Dickstein, "Unrolled Generative Adversarial Networks," *arXiv Preprint arXiv:1611.02163*, 2016.
- [49] Y. LeCun, "The MNIST Database of Handwritten Digits," <http://yann.lecun.com/exdb/mnist/>, 1998.
- [50] S. Ozair, C. Lynch, Y. Bengio, A. Van den Oord, S. Levine, and P. Sermanet, "Wasserstein Dependency Measure for Representation Learning," in *Advances in Neural Information Processing Systems*, 2019, pp. 15 604–15 614.
- [51] A. Srivastava, L. Valkov, C. Russell, M. U. Gutmann, and C. Sutton, "Veegan: Reducing Mode Collapse in Gans Using Implicit Variational Learning," in *Advances in Neural Information Processing Systems*, 2017, pp. 3308–3318.
- [52] T. Che, Y. Li, A. P. Jacob, Y. Bengio, and W. Li, "Mode Regularized Generative Adversarial Networks," *arXiv Preprint arXiv:1612.02136*, 2016.
- [53] Q. Mao, H.-Y. Lee, H.-Y. Tseng, S. Ma, and M.-H. Yang, "Mode Seeking Generative Adversarial Networks for Diverse Image Synthesis," in *Proceedings of the IEEE Conference on Computer Vision and Pattern Recognition*, 2019, pp. 1429–1437.
- [54] M. S. Sajjadi, O. Bachem, M. Lucic, O. Bousquet, and S. Gelly, "Assessing Generative Models via Precision and Recall," in *Advances in Neural Information Processing Systems*, 2018, pp. 5228–5237.
- [55] T. Kynkäänniemi, T. Karras, S. Laine, J. Lehtinen, and T. Aila, "Improved Precision and Recall Metric for Assessing Generative Models," in *Advances in Neural Information Processing Systems*, 2019, pp. 3929–3938.
- [56] P. Grnarova, K. Y. Levy, A. Lucchi, N. Perraudin, I. Goodfellow, T. Hofmann, and A. Krause, "A Domain Agnostic Measure for Monitoring and Evaluating GANs," in *Advances in Neural Information Processing Systems*, 2019, pp. 12 069–12 079.
- [57] P. Grnarova, K. Y. Levy, A. Lucchi, T. Hofmann, and A. Krause, "An Online Learning Approach to Generative Adversarial Networks," *arXiv Preprint arXiv:1706.03269*, 2017.
- [58] Y. Kim, M. Kim, and G. Kim, "Memorization Precedes Generation: Learning Unsupervised Gans with Memory Networks," *arXiv Preprint arXiv:1803.01500*, 2018.
- [59] S. Gidaris, P. Singh, and N. Komodakis, "Unsupervised Representation Learning by Predicting Image Rotations," *arXiv Preprint arXiv:1803.07728*, 2018.
- [60] X. B. Peng, A. Kanazawa, S. Toyer, P. Abbeel, and S. Levine, "Variational Discriminator Bottleneck: Improving Imitation Learning, Inverse RL, and Gans by Constraining Information Flow," *arXiv Preprint arXiv:1810.00821*, 2018.
- [61] N. Tishby, F. C. Pereira, and W. Bialek, "The Information Bottleneck Method," *arXiv Preprint Physics/0004057*, 2000.
- [62] H. Bhatia, W. Paul, F. Alajaji, B. Ghahserifard, and P. Burlina, "R\{e\}nyi Generative Adversarial Networks," *arXiv preprint arXiv:2006.02479*, 2020.
- [63] X. Mao, Q. Li, H. Xie, R. Y. Lau, Z. Wang, and S. Paul Smolley, "Least Squares Generative Adversarial Networks," in *The IEEE International Conference on Computer Vision (ICCV)*, Oct 2017.
- [64] S. Nowozin, B. Cseke, and R. Tomioka, "f-GAN: Training Generative Neural Samplers using Variational Divergence Minimization," in *Advances in Neural Information Processing Systems*, 2016, pp. 271–279.
- [65] D. Barber and F. V. Agakov, "The IM Algorithm: A Variational Approach to Information Maximization," in *Advances in Neural Information Processing Systems*, 2003, p. None.
- [66] "GANs with Spectral Normalization and Projection Discriminator," https://github.com/pfn-research/sngan_projection, accessed: 2019-10-31.

APPENDIX A SUPPLEMENTARY RESULTS

In this section, we detail supplementary results from various experiments done in the paper.

A. Evaluation Metrics Sample Sizes

For all FID scores reported in this paper, we compute them using 50K real samples and 10K fake samples across 3 random seeds to report the mean and standard deviation of the scores. As 50K real samples are much lesser than the 1.3M images in ImageNet, we randomly sample without replacement 50 images from each of the 1000 classes to compute the real image statistics, to avoid high bias in the results. We emphasize that for fairness in comparisons, we used the same number of real and fake samples when computing FID, since FID can produce highly bias estimates at different sample sizes [41]. In fact, we note that *lower FID scores* can indeed be obtained if we simply use larger sample sizes, particularly for larger datasets like ImageNet. However, our experiments show that in practice, the performance *margins* remain the same above our current configuration. For KID, we follow the same procedure for all datasets but use 50K real and fake samples instead. Finally, for IS, we use 50K fake samples.

We emphasize that all these evaluation settings are kept the same for all model evaluations, in order to ensure fairness and accuracy in our comparisons.

B. Generated Image Samples

For a qualitative comparison, we present randomly sampled, non-cherry picked images generated by SNGAN and InfoMax-GAN for all datasets in Figures 9, 10 and 11. We qualitatively observe that the images are more diverse and have sharper shapes after the use of an InfoMax objective.

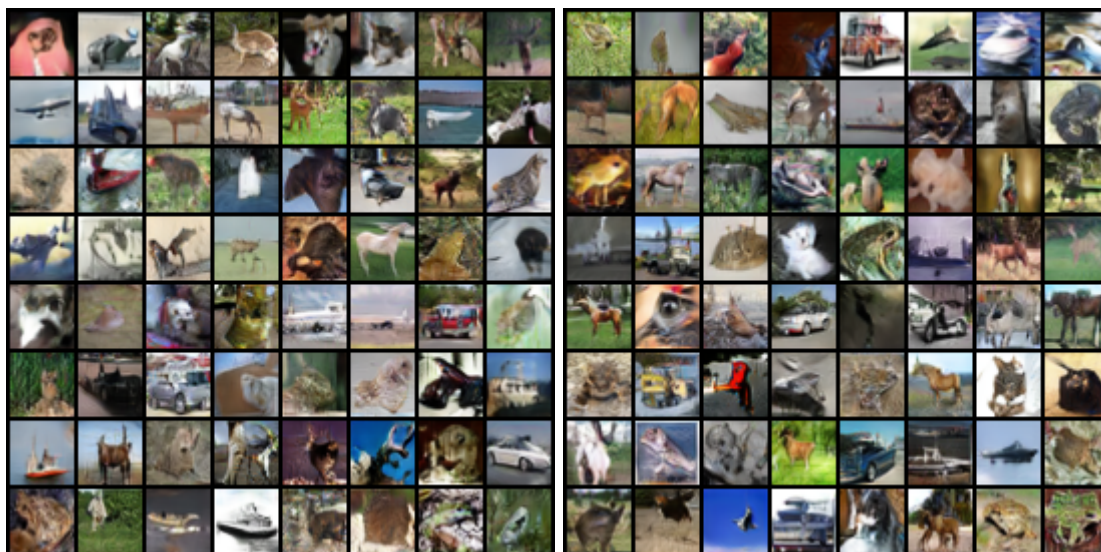
APPENDIX B INFOGAN COMPARISON

For clarity and disambiguity, Table VI illustrates the differences in our work with InfoGAN. Our works have different focuses: InfoGAN focuses on learning disentanglements in image generation, while we focus on improving image synthesis as a whole.

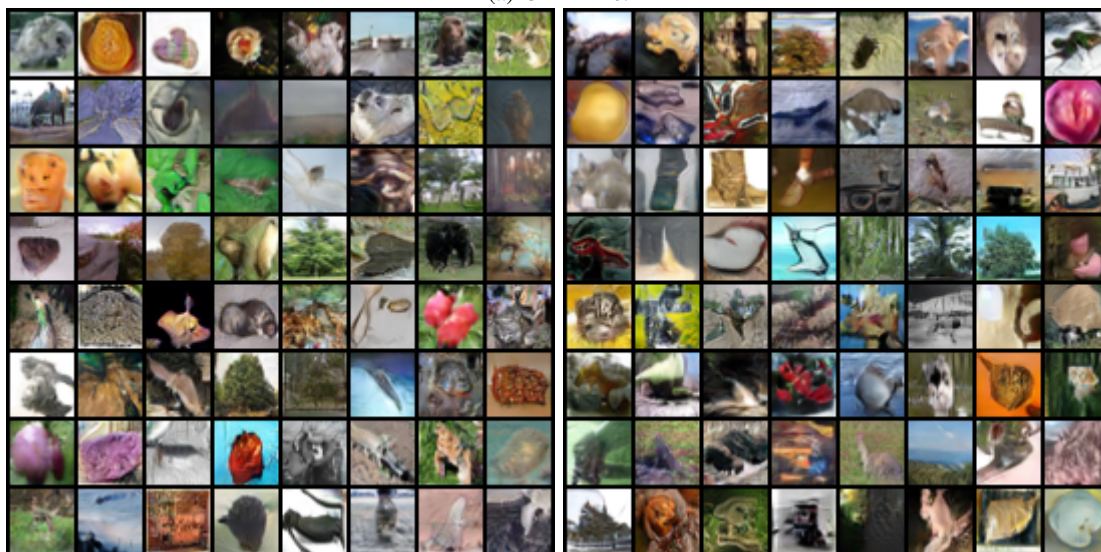
APPENDIX C MODEL ARCHITECTURES

We detail the exact GAN architectures used for all datasets in Tables VII, VIII, IX. We also detail the architectures for projecting the local and global features to a higher dimensional RKHS for solving the InfoNCE task in Table X.

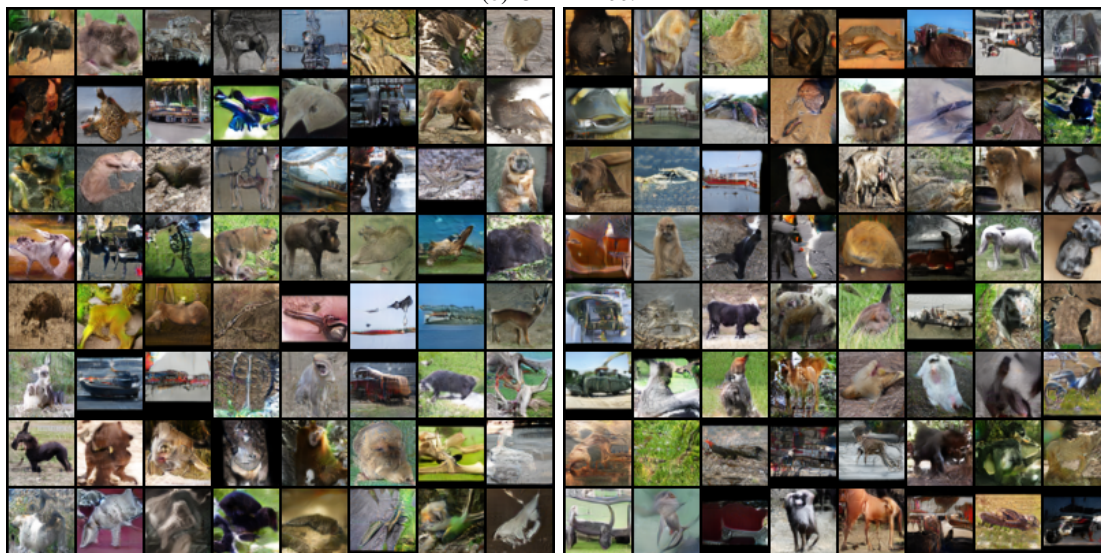
Fig. 9: Randomly sampled and non-cherry picked images for SNGAN (left) and InfoMax-GAN (right) for CIFAR-10, CIFAR-100, and STL-10.



(a) CIFAR-10.



(b) CIFAR-100.

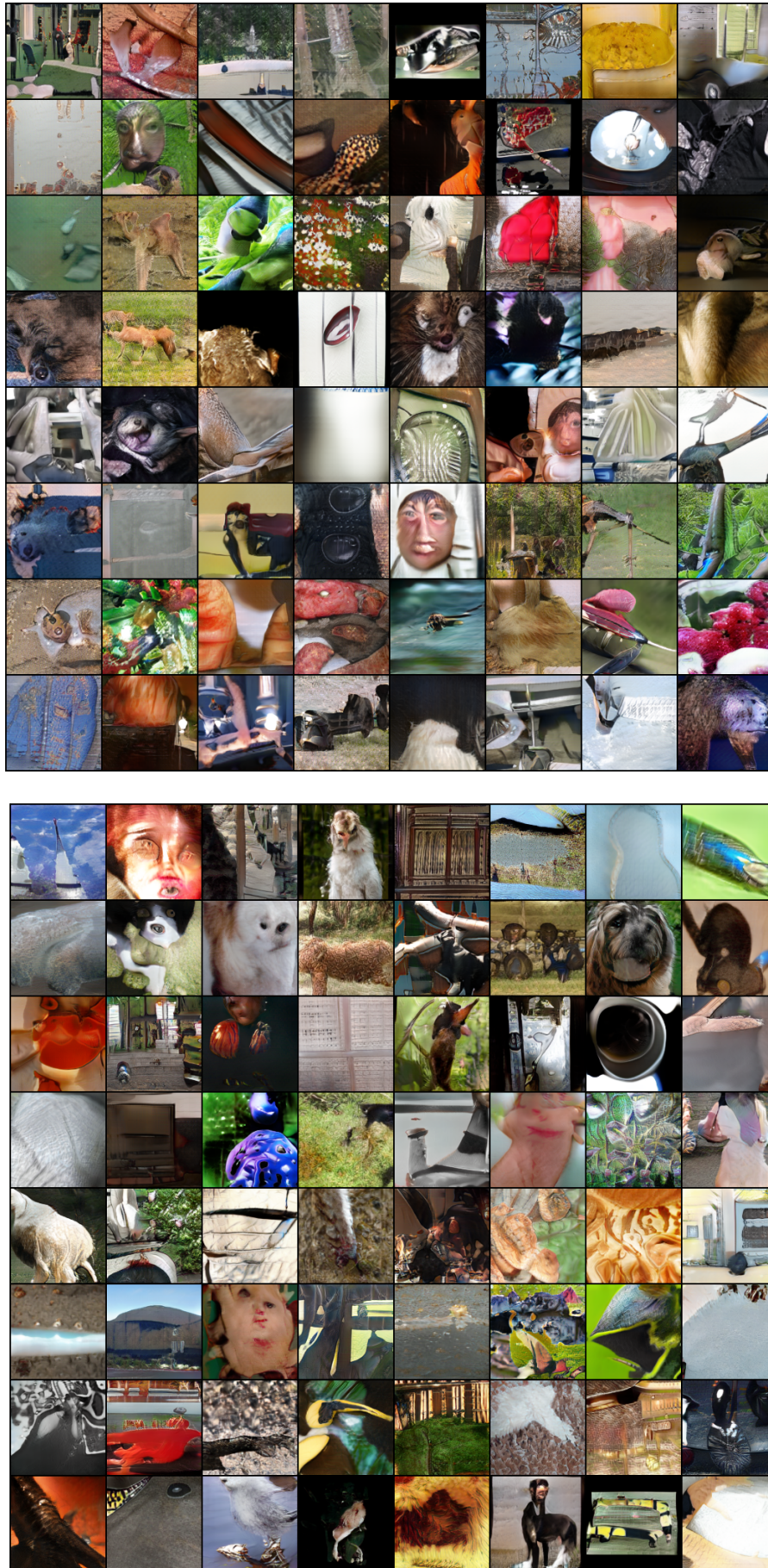


(c) STL-10.

Fig. 10: Randomly sampled and non-cherry picked generated CelebA images for SNGAN (top) and InfoMax-GAN (bottom).



Fig. 11: Randomly sampled and non-cherry picked generated ImageNet images for SNGAN (top) and InfoMax-GAN (bottom).



Work	Target Outcome	MI Objective	MI Approximation Technique
InfoGAN [40]	Disentangled representation learning by using an input encoding c to the generator to control its output.	$\mathcal{I}(c; G(z, c))$	Variational Information Maximization [65]
InfoMax-GAN (ours)	Improve image synthesis by reducing catastrophic forgetting of discriminator and mode collapse of generator.	$\mathcal{I}(C_\psi(X); E_\psi(X))$	InfoNCE [21] Task

TABLE VI: Comprehensive differences with InfoGAN. Our work mainly differs in the intended outcome, the objective to meet the outcome, and the approximation technique needed to solve the objective.

TABLE VII: Network architectures for the CIFAR-10 and CIFAR-100 datasets, which follows exact settings in [29].

(a) Generator	(b) Discriminator
$z \in \mathbb{R}^{128} \sim \mathcal{N}(0, 1)$	RGB image $x \in \mathbb{R}^{32 \times 32 \times 3}$
Linear, $4 \times 4 \times 256$	ResBlock down 128
ResBlock up 256	ResBlock down 128
ResBlock up 256	ResBlock 128 \rightarrow Local Features
ResBlock up 256	ResBlock 128
BN; ReLU; 3×3 conv, 3; Tanh	ReLU
	Global Sum Pooling \rightarrow Global Features
	Linear $\rightarrow 1$
(c) Self-supervised Discriminator	
RGB image $x \in \mathbb{R}^{32 \times 32 \times 3}$	
ResBlock down 128	
ResBlock down 128	
ResBlock 128 \rightarrow Local Features	
ResBlock 128	
ReLU	
Global Sum Pooling \rightarrow Global Features	
Linear $\rightarrow 1$; Linear $\rightarrow 4$	

TABLE VIII: Network architectures for the STL-10 dataset, which follows exact settings in [29].

(a) Generator		(b) Discriminator	
			RGB image $x \in \mathbb{R}^{48 \times 48 \times 3}$
	$z \in \mathbb{R}^{128} \sim \mathcal{N}(0, 1)$		ResBlock down 64
	Linear, $6 \times 6 \times 512$		ResBlock down 128
	ResBlock up 256		ResBlock down 256
	ResBlock up 128		ResBlock down 512 \rightarrow Local Features
	ResBlock up 64		ResBlock 1024
	BN; ReLU; 3×3 conv, 3; Tanh		ReLU
			Global Sum Pooling \rightarrow Global Features
			Linear $\rightarrow 1$
(c) Self-supervised Discriminator			
	RGB image $x \in \mathbb{R}^{48 \times 48 \times 3}$		
	ResBlock down 64		
	ResBlock down 128		
	ResBlock down 256		
	ResBlock down 512 \rightarrow Local Features		
	ResBlock 1024		
	ReLU		
	Global Sum Pooling \rightarrow Global Features		
	Linear $\rightarrow 1$; Linear $\rightarrow 4$		

TABLE IX: Network architectures for the CelebA and ImageNet datasets. This follows the exact settings in the official SNGAN code [66].

(a) Generator		(b) Discriminator	
$z \in \mathbb{R}^{128} \sim \mathcal{N}(0, 1)$		RGB image $x \in \mathbb{R}^{128 \times 128 \times 3}$	
Linear, $4 \times 4 \times 1024$		ResBlock down 64	
ResBlock up 1024		ResBlock down 128	
ResBlock up 512		ResBlock down 256	
ResBlock up 256		ResBlock down 512 \rightarrow Local Features	
ResBlock up 128		ResBlock down 1024	
ResBlock up 64		ResBlock 1024	
BN; ReLU; 3×3 conv, 3; Tanh		ReLU	
		Global Sum Pooling \rightarrow Global Features	
		Linear $\rightarrow 1$	
(c) Self-supervised Discriminator			
RGB image $x \in \mathbb{R}^{128 \times 128 \times 3}$			
ResBlock down 64			
ResBlock down 128			
ResBlock down 256			
ResBlock down 512 \rightarrow Local Features			
ResBlock down 1024			
ResBlock 1024			
ReLU			
Global Sum Pooling \rightarrow Global Features			
Linear $\rightarrow 1$; Linear $\rightarrow 4$			

TABLE X: InfoNCE projection architectures, which follow what were proposed in [22]. In practice, we extract the local features and global features from the penultimate and final residual blocks of the discriminator respectively. This decides the corresponding values of feature depth K .

(a) Local features projection architecture.	(b) Global features projection architecture.
1×1 Conv, K ; 1×1 Conv, $R \rightarrow$ Shortcut	Linear $\rightarrow K$; Linear $\rightarrow R \rightarrow$ Shortcut
ReLU	ReLU
1×1 Conv, $R +$ Shortcut	1×1 Conv, $R +$ Shortcut